Studies of African Wave Disturbances with the GISS GCM

LEONARD M. DRUYAN AND TIMOTHY M. HALL

NASA/Goddard Institute for Space Studies and Columbia University, New York, New York

(Manuscript received 21 August 1992, in final form 23 June 1993)

ABSTRACT

Simulations made with the general circulation model of the NASA/Goddard Institute for Space Studies (GISS GCM) run at 4° latitude by 5° longitude horizontal resolution are analyzed to determine the model's representation of African wave disturbances. Waves detected in the model's lower troposphere over northern Africa during the summer monsoon season exhibit realistic wavelengths of about 2200 km. However, power spectra of the meridional wind show that the waves propagate westward too slowly, with periods of 5–10 days, about twice the observed values. This sluggishness is most pronounced during August, consistent with simulated 600-mb zonal winds that are only about half the observed speeds of the midtropospheric jet. The modeled wave amplitudes are strongest over West Africa during the first half of the summer but decrease dramatically by September, contrary to observational evidence. Maximum amplitudes occur at realistic latitudes, 12°–20°N, but not as observed near the Atlantic coast. Spectral analyses suggest some wave modulation of precipitation in the 5–8-day band, and compositing shows that precipitation is slightly enhanced east of the wave trough, coincident with southerly winds. Extrema of low-level convergence west of the wave troughs, coinciding with northerly winds, were not preferred areas for simulated precipitation, probably because of the drying effect of this advection, as waves were generally north of the humid zone. The documentation of African wave disturbances in the GISS GCM is a first step toward considering wave influences in future GCM studies of Sahel drought.

1. Introduction

An early description of African wave disturbances with periods of generally 3–5 days is given by Burpee (1972), based on spectral analyses of tropospheric meridional winds observed at selected stations in northern Africa. He attributes their generation to the vertical and horizontal shear created by the African easterly jet (AEJ) at 700 mb. Norquist et al. (1977) suggest that these waves form as a consequence of combined baroclinic and barotropic instability. Barotropic instability is generated by horizontal shear associated with the AEJ (Burpee 1971), which is well developed over northern Africa during boreal summer between 15°E and 20°W, also the favored region for these easterly waves (Hastenrath 1988). The meridional temperature gradient, which is strengthened over the Sahel region during early summer as the cool Atlantic monsoon air mass is thrust northward against hot Sahara air, also creates vertical shear in the zonal wind, a source of wave energy that can grow through baroclinic instabilities.

The typical structure of such waves includes 200-mb divergence associated with the tropical easterly jet (TEJ) west of the axis of the midtropospheric wave and directly over the precipitation bands (Reed et al. 1977). Variations in the strength of the TEJ and related 200-mb divergence are positively correlated with interannual variations in seasonal Sahelian precipitation (Kidson 1977; Newell and Kidson 1984), perhaps because upper-tropospheric divergence regulates the intensity of vertical motion and therefore the rain-generating effectiveness of African waves. In addition, Newell and Kidson (1984) showed observational evidence that the AEJ is stronger during summer droughts in the Sahel. Rowell et al. (1992) found a positive correlation between Sahel seasonal rainfall and the seasonal mean latitude of the AEJ in GCM simulations, which they attributed to latitudinal fluctuations of midtropospheric moisture convergence "tied" to the north side of the jet. Since the energy of African wave disturbances is derived from the shear created by the AEJ (Burpee 1972; Norquist et al. 1977; Hastenrath 1988), the variability of the waves' intensities and the variability of the latitude of the waves' trajectories could be sources of some of the interannual variability of Sahel precipitation.

The genesis of African wave disturbances depends on the characteristics of the midtropospheric AEJ, while latent heat release in organized convection plays an important role in their growth and maintenance over West Africa (Norquist et al. 1977). The positive vertical motion in areas of deep convection, in turn, may be related to the divergence at 200 mb generated by the TEJ (Duvel 1990; Landsea and Gray 1992). Lamb and Peppler (1991, 1992) note that the 1983

Corresponding author address: Dr. Leonard M. Druyan, NASA/Goddard Institute for Space Studies, Columbia University, 2880 Broadway, New York, NY 10025.

Sahel drought was not associated with the typical SST anomaly patterns identified for other drought years, and they suggest that teleconnections from the strong El Niño signal in the Pacific Ocean may have suppressed squall-line activity over West Africa. The eastward displacement of the TEJ during the summer of 1983 has been cited as the cause of weakened divergence at 200 mb and the corresponding weakened intensity of rain-producing squall lines over the Sahel (see World Meteorological Organization 1985). Similarly, Ratcliffe (1989a,b) reported that the TEJ of 1988 had recovered from its former weakness following the 1987 El Niño and precipitation over sub-Saharan Africa registered its first relatively rainy season in many years.

Significant rainfall over West Africa is often associated with African wave disturbances. The composite of eight African waves analyzed by Reed et al. (1977) includes a precipitation maximum to the southwest of the wave apex and a relative minimum to the southeast. Payne and McGarry (1977) found that enhanced convective cloud cover associated with large cloud clusters occurred most often immediately west of the 700-mb wave trough during 28 days in August–September 1974. Genesis of a squall-line cloud cluster over West Africa studied by Fortune (1980) occurred east of a 700-mb wave trough, but experienced rapid growth when it caught up with the trough line some 12 h later. Individual squall-line arcs continued to run ahead of the trough where they eventually dissipated. In their study of midtropospheric waves over the Atlantic Ocean adjacent to West Africa, Chen and Ogura (1982) found somewhat different wave category/rainfall relationships for the different summer phases of GATE (GARP Atlantic Tropical Experiment), but the trough was usually favored for heavy precipitation. Duvel (1988) determined that more than 70% of the interdiurnal variance of summer convection is accounted for by spectral periodicities of 1–8 days, an interval that includes the periods of observed African wave disturbances (Reed et al. 1977; Reed et al. 1988).

Albignat and Reed (1980) showed spatial distributions of spectral amplitudes of 2.5–5-day-period oscillations in the meridional wind component at 850 and 700 mb over West Africa and the adjacent Atlantic using GATE Phase III data (23 August–19 September 1974).

More recently, Duvel (1990) compared wind analyses from the ECMWF (European Centre for Medium-Range Weather Forecasts) model with Meteosat IR estimates of convective activity to study the modulation of occurrences of deep convection by African wave disturbances for the drought summers of 1983, 1984, and 1985. In agreement with the Reed et al. (1977) composite, he found maxima of deep convection at and ahead (west) of 850-mb wave troughs near 7.5°N related to maxima in low-level convergence and 200-mb divergence.

However, Duvel's analysis showed greater spectral amplitudes and stronger convergence and vorticity associated with wave activity closer to 17.5°N. Moreover, in this region the maxima of deep convection were positioned behind (to the east of) the trough, coinciding with surges of northward-penetrating moist monsoon air. At and ahead (west) of the trough near 17.5°N, strong low-level convergence did combine with 700-mb divergence to produce intense upward vertical motion, as in the Reed et al. (1977) model. However, owing to the very low moisture content of the lower troposphere in this category of the wave, which is characterized by the southward advection of extremely dry Sahara air, the convection was mostly dry with little cloudiness or precipitation.

Composites by Burpee (1974), using northern Africa station data for the summers of 1968 and 1969, reported similar results. He found that the wave trough defined by surface winds was favored for precipitation in the south, between 6.5° and 12.5°N, but not further north, between 12.5° and 21.5°N, where the maximum was east of the trough.

Since each of the observational studies was somewhat limited in its spatial or temporal scope, we do not yet have a clear picture regarding the interannual variability of latitudinal, seasonal, or large-scale dynamics influences on the properties of African wave disturbances and their associated rainfall.

GCM (general circulation model) experiments have an excellent potential for investigating the impact that the interannual variability of the mid- and upper-tropospheric jets may have on the frequency and intensity of the easterly waves and their associated precipitation over West Africa. Many studies have used GCMs to test theories of surface influences, such as sea surface temperature, ground moisture, and land albedo on the interannual variability of Sahel rainfall (Druyan 1991; Rowell et al. 1992; review in Druyan 1989). However, none of this model-oriented research has considered the role of the African wave disturbances. The present study represents a first step toward this goal by offering documentation of one GCM's representation of the phenomenon.

Easterly waves have been previously studied with GCMs in other contexts. Miyakoda and Sirutis (1977) estimated trough and ridge positions of tropical easterly waves from 850-mb winds simulated by a GFDL (Geophysical Fluid Dynamics Lab) GCM with 3.75° horizontal resolution and Reed et al. (1988) documented the performance of the ECMWF operational system in analyzing and forecasting easterly waves over West Africa and the tropical Atlantic Ocean.

There is great interest in the mechanisms causing interannual variability of Sahel precipitation, and the investigation of African wave disturbances may provide some clues. In this paper we describe the representation of these waves in the GCM of the NASA/Goddard Institute for Space Studies (GISS). The intraseasonal

and spatial variations of wave activity are analyzed, as is the influence of this activity on divergence and precipitation.

2. The model

For the purposes of this study, the GISS GCM was run at the horizontal resolution of 4° latitude by 5° longitude, a resolution adequate for resolving wavelengths on the order of 2000 km. The basic equations are integrated at nine vertical levels. Model structure and performance were described by Hansen et al. (1983), the verification of regional circulation features during June–August is reported by Druyan and Rind (1989), and aspects of the modeled African summer monsoon are shown by Druyan (1987). Additional diagnostics for runs at 4° × 5° resolution have been published by Rind (1987, 1988), while Druyan (1992) discusses simulations at 4° × 5° resolution that were forced with globally observed SST.

The GCM has nine vertical levels and a fully active ground hydrology that keeps track of heat and moisture storage in the ground surface. Computed clouds interact with the modeled solar and terrestrial radiation transfer, and moisture, sensible heat, and momentum are transported vertically by convection. A simple mass flux cumulus parameterization (Del Genio and Yao 1993) is utilized whereby moist convection is diagnosed to occur whenever a parcel of air lifted adiabatically from some level is buoyant with respect to the environment at the next higher level. From there the parcel rises to the highest contiguous level at which buoyancy still exists. A fixed 50% of the mass of the cloud-base layer rises in each event, without additional entrainment into the rising plume. Heating of the environment results from compensating subsidence, and cooling from reevaporation of falling precipitation.

3. Mean circulation

Figure 1 shows latitude–height cross sections of the June, July, August, and September monthly mean zonal winds from a three-run ensemble averaged over 7.5°W–2.5°E. In June, the midtropospheric jet is es-

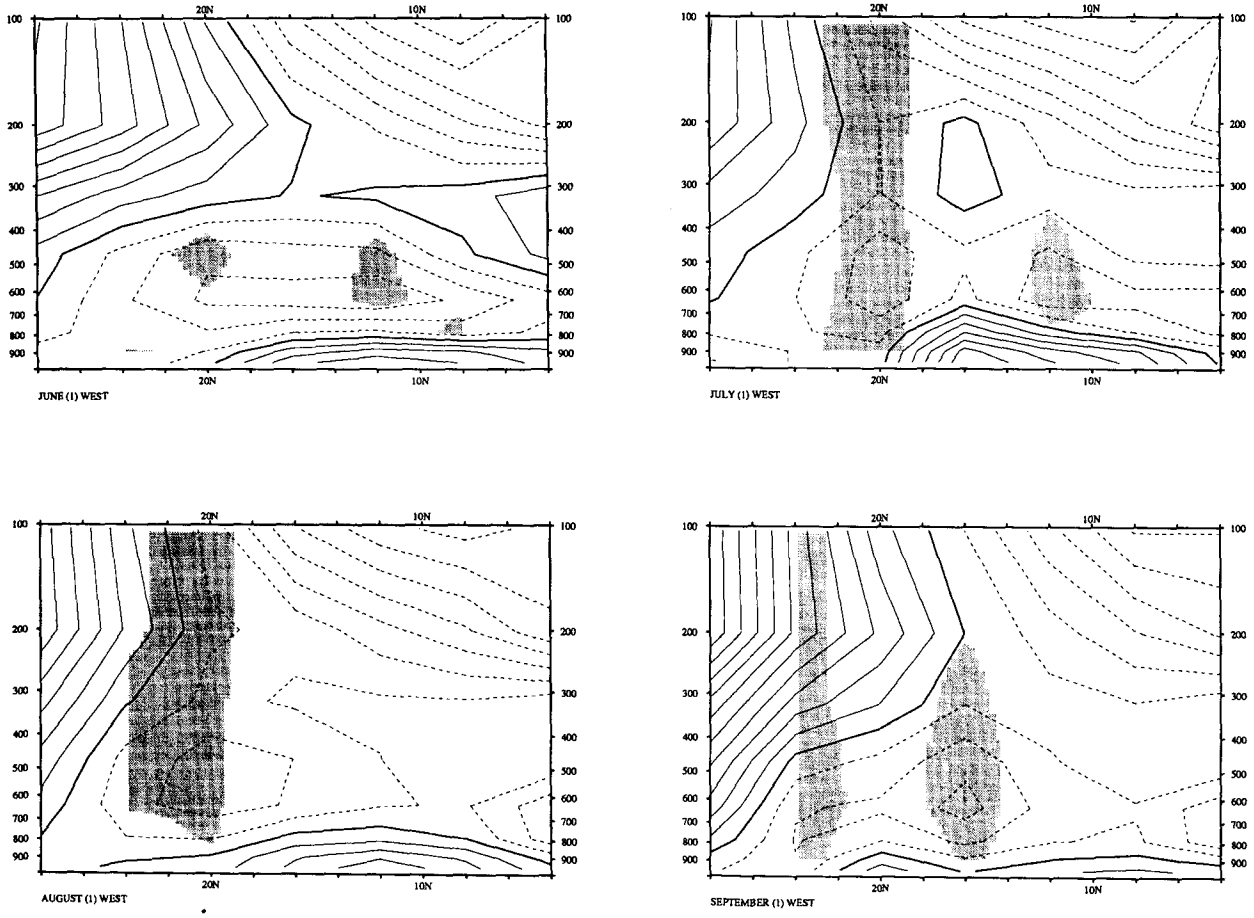

FIG. 1. Latitude–height cross sections of zonal winds for June, July, August, and September averaged between 7.5°W and 2.5°E, first ensemble. Shading indicates regions where the meridional gradient of the potential vorticity (based on the zonal winds) is negative. Contour interval 3 m s^{-1}, broken contours indicate negative values (easterly winds).

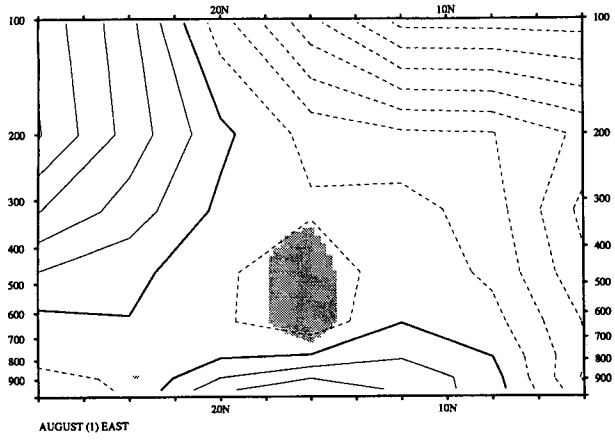

FIG. 2. Latitude–height cross section of zonal winds for August averaged between 22.5° and 32.5°E, first ensemble. Shading indicates regions where the meridional gradient of the potential vorticity (based on the zonal winds) is negative. Contour interval 3 m s^{-1}, broken contours indicate negative values (easterly winds).

tablished at about 600 mb, centered near 16°N, while a more distinct but weaker core forms over 20°N in July and August. In September, the core of maximum easterlies regains strength as it retreats to 16°N. The August cross section captures the general features depicted by comparable representations of the observed August zonal winds over West Africa (Burpee 1972; Reed et al. 1977; Newell and Kidson 1984). The core speed of the modeled AEJ in August is, however, some 5–10 m s^{-1} too slow and about 5° latitude too far north compared with observations. In the cross section of zonal winds for August of a second ensemble (not shown), core speeds of the midtropospheric jet are similar to first-ensemble values, but extend from 12° to 20°N, more in line with observational evidence. Given the importance of the AEJ in the formation of African wave disturbances, discrepancies in the modeled core speed and/or latitude can be expected to adversely affect the model's representation of the waves.

Burpee (1971, 1972) and Reed et al. (1977) found that the criterion for instability (Charney and Stern 1962) is satisfied near the AEJ (10°–24°N) as represented by time mean latitude–height distributions of the zonal wind. Burpee's (1972) computations of the meridional gradient of potential vorticity at 700 mb based on these data additionally showed that both horizontal and vertical shears of the zonal wind make significant contributions to these instabilities, which are important sources of energy for African wave disturbances. Since the criterion for instability requires that the isentropic gradient of the potential vorticity disappears, regions where the usually positive gradient becomes negative are thought to be favorable for wave development. Shading indicates such regions of instability on the cross sections in Fig. 1 based on computations with the modeled ensemble mean zonal winds. Note that June, July, and August all show instabilities associated with the AEJ near 20°N, at the northern extreme of where they have been computed from observations, while the shaded areas in September are at 16°N and north of 22°N.

It is clear from the extent of the shaded regions that the modeled AEJ, although weaker than observed, nevertheless provides enough horizontal and vertical shear to satisfy the Charney–Stern (1962) criterion for barotropic and baroclinic instabilities responsible for midtropospheric wave growth. Since time and ensemble averaging weaken gradients, we surmise that the instantaneous distributions of simulated winds probably generate strong instabilities over even broader areas.

Figure 2 shows a latitude–height cross section of the modeled zonal wind averaged over 22.5°–32.5°E. The August distribution shows a center of weak midtropospheric easterlies that compares favorably to observations along 35°E shown by Burpee (1972), who found instabilities there only during August. The shading on Fig. 2 indicates that wind shear associated with these easterlies is sufficiently strong to give rise to baroclinic/barotropic instabilities near 16°N. Contrary to Burpee's (1972) findings, instabilities were also detected from the zonal wind cross sections at this longitude for June, July, and September.

4. GCM depiction of waves

Meridional and zonal winds at 890 and 780 mb and the precipitation rate were saved as 6-h averages at 84 grid locations over northern Africa in each of six model simulations, from 1 June to 6 October. The six simulations, each begun from a different observed initial atmospheric state, comprise two ensembles of three runs each, where the runs making up each ensemble used the same global SST dataset.

a. Wind fields

Inspection of plotted six-hourly resultant wind vectors at both model levels revealed many examples of westward-propagating cyclonic circulations with wavelengths of 2000–2500 km. Figure 3 shows a four-day sequence of streamflow analyses of model 780-mb winds over northern Africa during early October, based on vectors of the resultant winds for the first 6 h of each day shown. The analyses show a wave that advances from 5°W to 15°W by the fourth day, for an average westward wave speed of approximately 3.3 degrees longitude per day, compared with an average speed of 6–7 degrees per day for the waves analyzed by Reed et al. (1977).

Figure 3 and similar analyses for other parts of the season (not shown) also suggest some modulation of the daily precipitation rate by the waves that are present. Note that on days 123 and 125, for example, precipitation favors the east side of the trough axis and

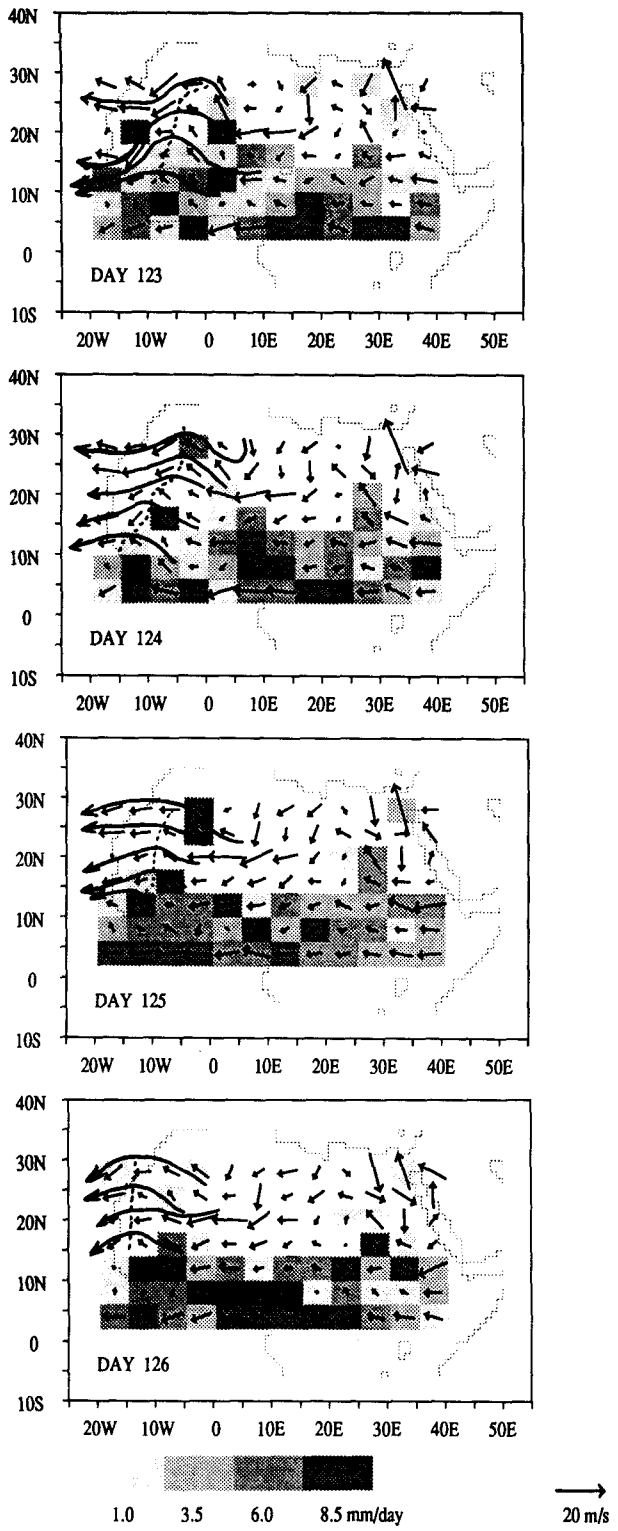

FIG. 3. Daily sequences of circulation patterns based on model 780-mb 6-hourly resultant winds. Trough axes of modeled waves are highlighted by interrupted line segments. Shading indicates the mean precipitation rate (mm day^{-1}) for the first 6 h of each day according to the accompanying gray scale.

therefore, southerly circulation. The alignment of rainfall east of wave troughs recalls Duvel's (1990) findings for West Africa between 13° and 22°N. This matter is further addressed below.

Figure 4 shows the spatial distribution of the linear correlation coefficient (R) between time series of the 780-mb meridional wind (v) at 16°N, 2.5°W and the "v" time series at the remaining grid elements over northern Africa, for each month, averaged over all six runs. (The "v" were first passed through a 2–16-day bandpass filter.) To evaluate the significance of these R, linear correlations were computed between the "v" series and random series undergoing identical postprocessing. The random series were designed to have statistical properties (lag-one autocorrelations) similar to the GCM output. The standard deviation about the overall zero mean of the test correlations between these series was only about 0.15, indicating the significance of the R contoured in Fig. 4. Relatively large negative R at 10° longitude east and west of the reference longitude in each month indicate that northerlies (southerlies) are favored at these locations whenever southerlies (northerlies) occur at 2.5°W, implying periodic perturbations with wavelengths of about 2200 km, similar to previous estimates of African wave disturbances (Reed et al. 1977; Reed et al. 1988). In addition, the north–south symmetry of the pattern indicates that the traversing waves span some 8°–16° latitude. The very weak correlations for September indicate only marginal spatial coherence of the wave pattern near the end of the season, contrary to observational evidence.

b. Power spectra of meridional wind (v)

We computed power spectra from time series of the 6-h mean wind components at model levels 2 and 3. Figure 5 shows some examples of these power spectra, averaged over the three runs of the first ensemble, based on 32-day (detrended) time series (beginning 1 June) of v along 7.5°W and 2.5°W. A narrow peak occurring at the diurnal frequency is especially strong over the northerly (desert) latitudes. In addition, there is significant power at very low frequencies, corresponding to a 2–4-week variability reflecting intraseasonal evolution. In general, the spectra tend to be "red," consistent with Burpee's (1972) observational studies. However, Fig. 5 also shows prominent peaks in the 5–8-day band that stand above the reddish spectra, and we attribute these peaks to model-simulated African waves. In power spectra for July and August (not shown), on the other hand, peaks concentrate in the 7–10-day range. The intraseasonal variation of the predominant periods is discussed in section 4c.

The 5–10-day periodicities of these GCM-generated perturbations are longer than those described by previous studies, although Burpee (1972) did show a rather broad spectral maximum of 5–7 days in the meridional

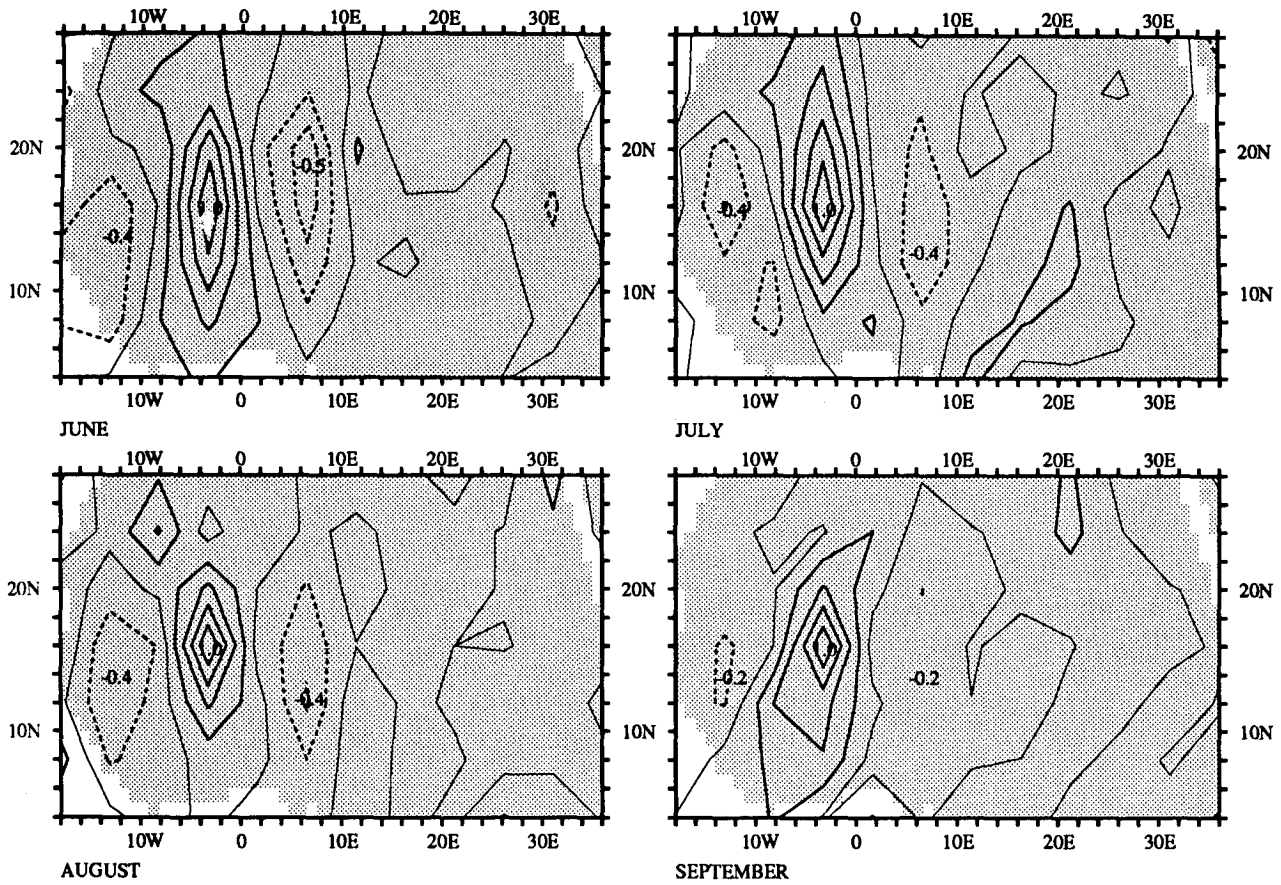

FIG. 4. Correlation coefficients between 6-hourly mean meridional components of 780-mb winds at 16°N, 2.5°W and the other grid points over northern Africa, averaged for each month over six simulations. Contributions to the wind components from periods less than 2 days and greater than 16 days have been filtered.

wind observed at 700 mb over Dakar (14°N, 17°W) for June 1960–64. Additionally, Burpee (1972) suggested that wave periods derived from spectral analysis could be slightly larger than those obtained by tracking individual waves on synoptic charts because time series of the winds include frequent interruptions of wave activity and variations of amplitude between successive waves. This notwithstanding, the 7-day periods of the modeled waves undoubtedly reflect the influence of a weaker midtropospheric easterly wind maximum than is observed (Fig. 1).

The 5–8-day peaks in the v spectra apparent in Fig. 5 are indeed caused by the westward propagation of the same waves whose 2200-km length can be deduced by examination of Fig. 4. To demonstrate this, coherence squared spectra (magnitude squared of the normalized cross product of two frequency spectra) were formed between one-month time series of v (level 3) at adjacent grid elements. Figure 6a shows very well defined coherence peaks reaching near 0.7 at about the 6-day period between 5° longitude-displaced series of v along 16°N and 20°N. This high coherence indicates that the variations of these neighboring v time series have a fixed phase relationship at this frequency. Moreover, Fig. 6a shows that the relative phase at the 6-day peaks in this case is +90°, indicating that the signal to the east leads the one 5° to the west by one-quarter of a wavelength, consistent with our interpretation of Fig. 4. Coherence spectra for the 4° latitude-displaced time series of v (Fig. 6b) identify waves of the same period, but indicate almost no phase lag in the latitudinal direction. Note that the coherent diurnal (1-day period) impulses at adjacent grid elements are also generally in phase, as one would expect. Consistent with the above, coherence spectra between 10° longitude-displaced time series of v show peaks of 0.3–0.5 and phase lags of ±180° (Fig. 6c).

c. Spatial distribution of wave amplitudes

Figure 7 shows the spatial distribution of spectral amplitudes in the 5–8-day bands for 780-mb meridional winds over all 84 grid elements over northern Africa for each quarter of the season (roughly corresponding to the calendar months June, July, August, and September) and for each ensemble. These distri-

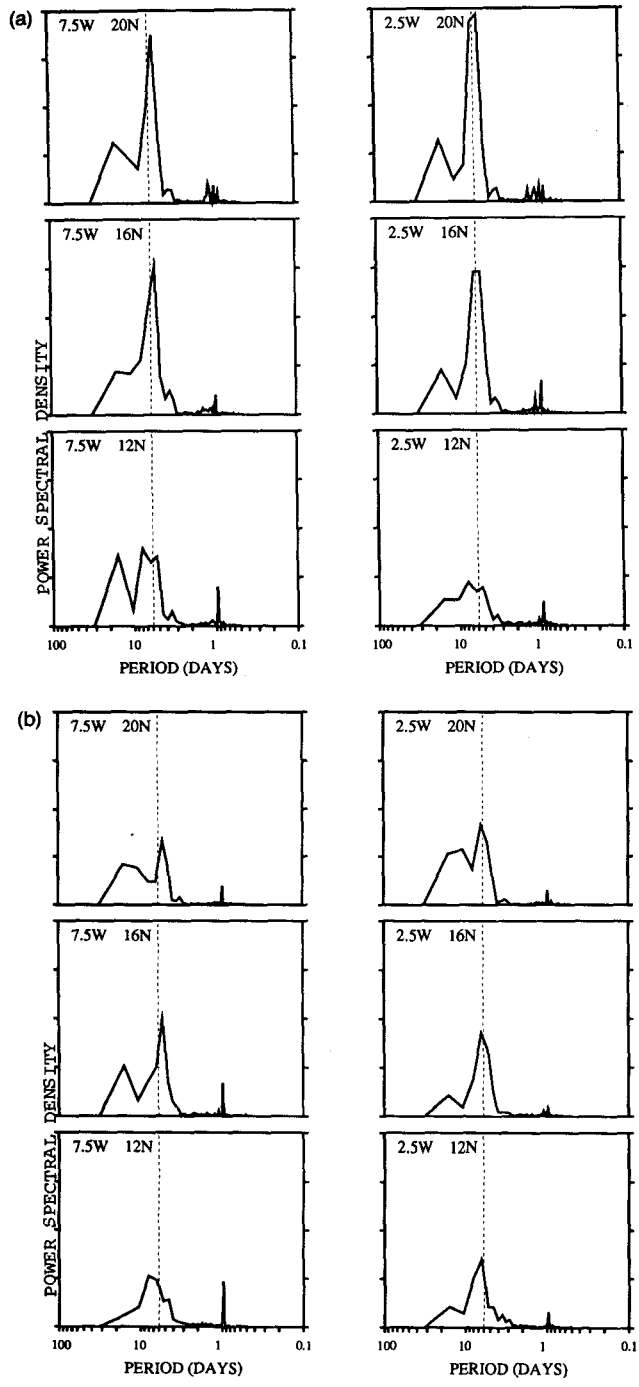

FIG. 5. Power spectra of 6-hourly mean meridional winds for June of the first ensemble at selected grid elements: at 890 mb (a) and 780 mb (b). The reference line indicates 6-day periods.

butions can be compared to similar mappings based on 23 August–19 September 1974 wind data by Albignat and Reed (1980) and those based on analyzed 1983–1985 ECMWF winds by Duvel (1990). Maximum amplitudes between 0° and 10°W occur close to 20°N (15°N) at 850 mb (700 mb) in Duvel's (1990) representation but are some 8° latitude farther south according to the 1974 data (Albignat and Reed 1980), reflecting some measure of interannual variability or limitations of the analyses in data-sparse areas of northern Africa. The model results depicted in Fig. 7 indicate maximum amplitudes generally between 16° and 20°N, closer to the 1983–85 example, and both the model results and Duvel's empirical study imply decreases in wave activity southward to the Gulf of Guinea coast and southeastward toward the Sudan and Ethiopia. The two observational studies also indicate amplitude maxima along the Atlantic coast between 10° and 20°N, while Fig. 7 displays a conspicuous absence of strong wave amplitudes along 12.5°–17.5°W, the westernmost longitudes considered. On the other hand, a comparable analysis based on surface winds from June–September 1968 and 1969 (Burpee 1974) does not show the coastal maximum either, but this may be more a consequence of the near-surface conditions than interannual variability. The relative minimum of wave activity along the Atlantic coast in the GISS GCM simulations may indicate that modeled waves moving toward the coast are not being strengthened through the organized release of latent heat from moist convection, a mechanism suggested by several investigators (Norquist et al. 1977; Kwon 1989).

Wave amplitudes for both model ensembles are greatly reduced in September, at variance with the observational evidence (Burpee 1972; Albignat and Reed 1980; Duvel 1990). Although Duvel's (1990) analysis indicates slight decreases of wave amplitude at 850 mb, and greater decreases at 700 mb, between the first and second halves of the summer east of 0° longitude, increases west of 0° are quite pronounced. Burpee (1972) found that August experiences a relative minimum in the 700-mb spectral amplitude of African waves over Dakar (14°N on the Atlantic coast), but his data show a significant increase in September. Miller and Lindzen (1992) suggest that higher atmospheric levels are more appropriate for monitoring wave characteristics in August when the core of the AEJ reaches its highest altitude. Figure 1 shows that the retreat of the modeled AEJ between August and September is accompanied by a shift of the instability region from 20°N to a narrower region over 16°N, offering little explanation for the September minimum in wave amplitudes.

We found that the relatively low amplitudes shown in Fig. 7 for September reflect the fact that the generation of wave activity moves southward (of 16°N), where the total variance of the modeled meridional wind decreases dramatically compared to August. Figure 8 shows the spatial distribution of the power of "v" at 780 mb, integrated over the 5–8-day period interval for September, expressed as a percent of the power integrated over the entire spectrum. It indicates that this spectral interval accounts for a maximum of more than 40% of the total spectral power over an area of West Africa centered on 12°–16°N, 2.5°W, close to

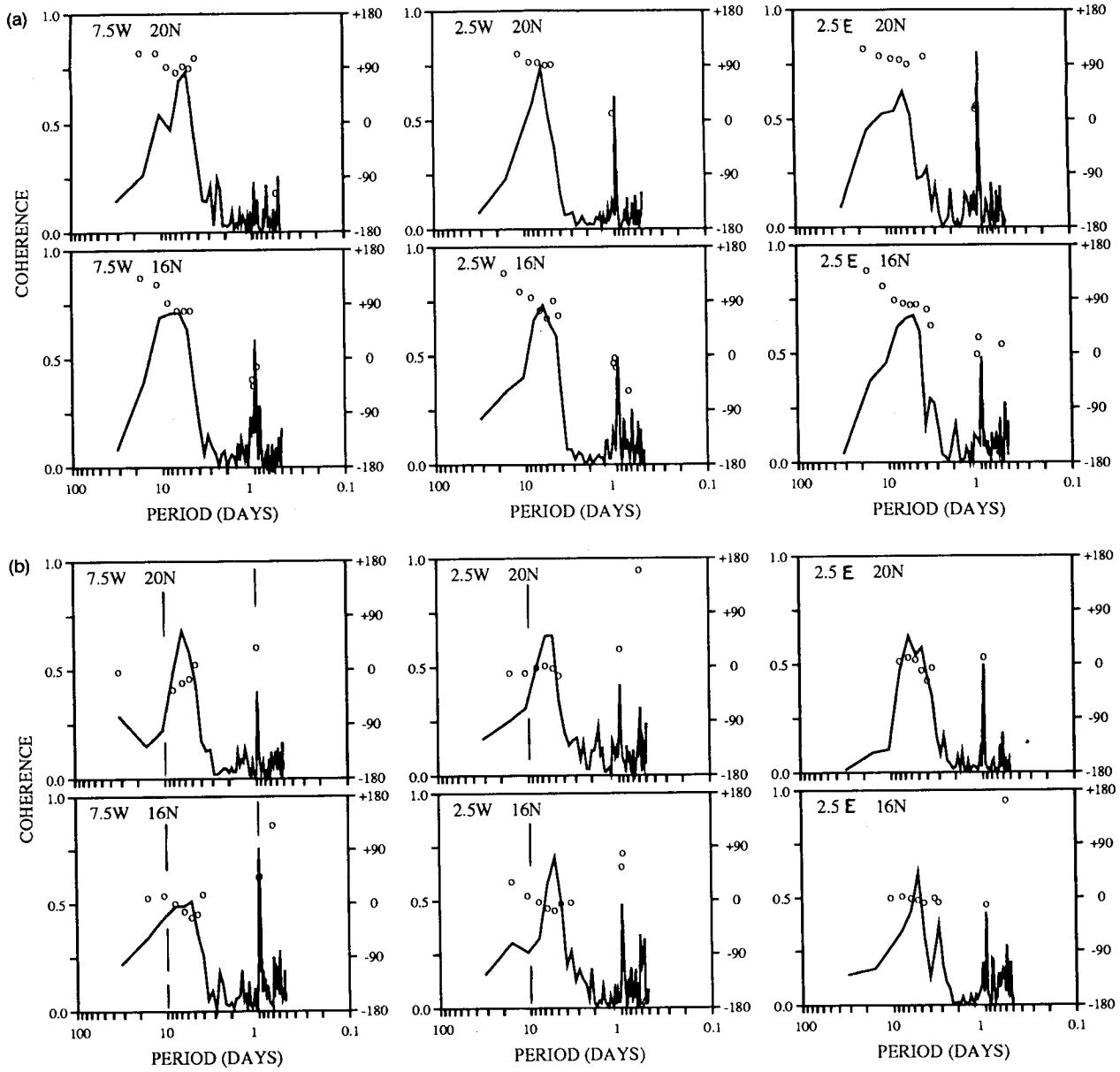

FIG. 6. Coherence spectra between one-month time series of the meridional wind (780 mb) at selected paired grid elements. Circles indicate the relative phase at a particular period, plotted (for coherence >0.25) according to the right-hand scales. Spectra are averages based on all 24 months of model simulations. (a) Coherence spectra between the v series at the indicated grid element and the adjacent element 5° to the west. (b) Coherence spectra between the v series at the indicated grid element and the adjacent element 4° to the south.

the AEJ position in September (Fig. 1). Spatial distributions for the other months (not shown) indicate similar maxima of the relative power in the 5–8-day period band over West Africa, but farther north, consistent with the seasonal migration of modeled AEJ latitude. In addition, by mapping the relative power of "v" for other intervals, we determined that predominant periods of wave power shift from 4.6 to 6.4 days in June, upward to 8 to 10 days in August, and back to lower periods in September. This intraseasonal variation reflects the slowing of wave phase speeds by the weaker mean easterlies in the GCM during August.

Some interannual differences are evident from a comparison of the two ensembles. For example, ensemble 1 shows a closer resemblence to Duvel's (1990) distribution regarding the northeast–southwest orientation of maximum amplitudes in June and July.

It is conceivable that some of the differences between these spatial distributions of wave amplitude and the distributions given by Duvel (1990) are related to the

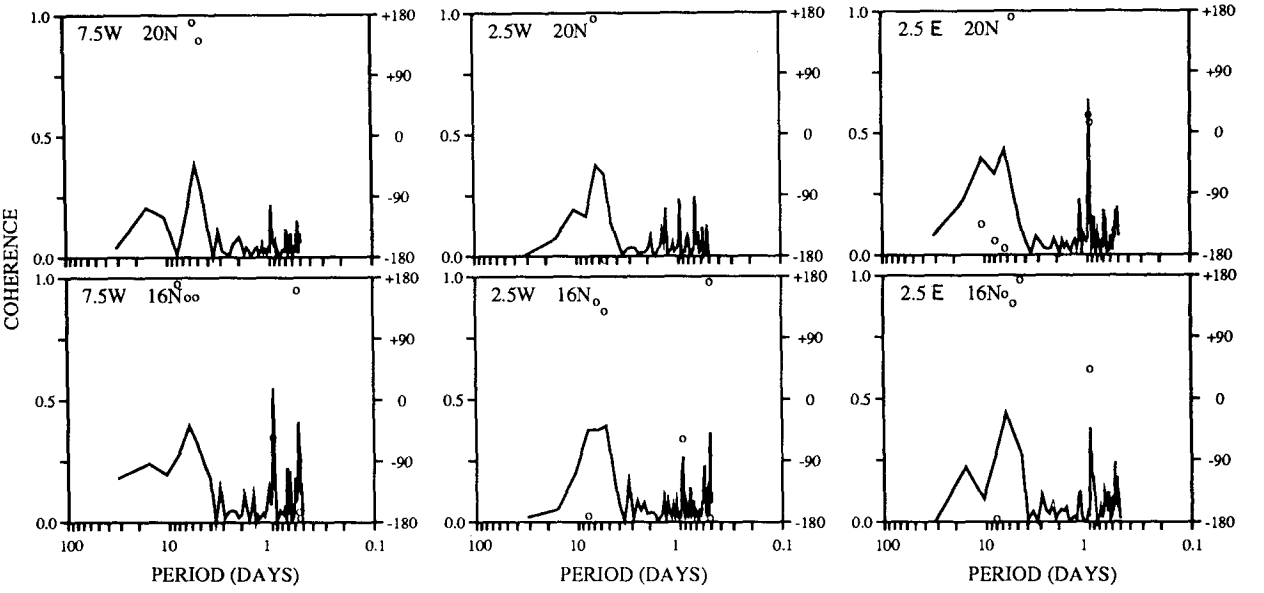

FIG. 6. (*Continued*) Coherence spectra between the v series at the indicated grid element and the element 10° to the west.

contrasts between the GISS GCM simulations and the ECMWF operational analysis system, including the biases of each model. There is, however, probably considerable interannual variability in this field as reflected by the differences between the depictions by Duvel (1990) and those of Albignat and Reed (1980). We also note that Duvel used data from 1983, 1984, and 1985, which were seasons with rather severe droughts in the Sahel, so his analyses are more representative of anomalous conditions than the mean climate.

5. Wave modulation of precipitation

a. Seasonal march of rainfall

Figure 9 shows the June and August distributions of monthly mean precipitation rate for the first simulation ensemble. Note that heavier precipitation spreads northward during the first half of the summer, except along the Atlantic coast. Figure 9 also shows that this northward advance is related to the expanding area of horizontal moisture flux convergence, which increases midtropospheric specific humidities by 5%–12% at 14°N between June and August (not shown). In June, very little rainfall occurs at 15°–20°N, the latitudes of maximum wave amplitude (Fig. 7). By August, however, the 3 mm day^{-1} isohyet has already reached 20°N, where considerable wave amplitude is still in evidence.

b. Power spectra

Figure 10 shows power spectra of 6-h mean precipitation rate time series at selected grid elements along 22°N and 18°N, averaged for August–September of both ensembles. As in the wind spectra, the diurnal forcing shows up as sharp peaks corresponding to 1-day periods, and the spectra are fairly noisy otherwise. However, 8-day peaks can also be discerned at 18°N, 10° and 5°W, and weaker 5–6-day peaks at 22°N, 10°W and 0°. This evidence of 5–8-day periods in the precipitation spectra suggests a wave modulation of modeled rainfall at certain grid locations.

Figure 11 shows coherence squared spectra (magnitude squared of the normalized cross product of two frequency spectra) between the 6-h mean v (780 mb) and 6-h means of the precipitation rate for August and September for all six simulations. Values of coherence greater than 0.20 are significant at the 99% confidence level. At the two grid locations with sharp precipitation spectra peaks at 7–8-day periods (Fig. 10), coherence peaks of 0.5–0.7 occur for the same spectral frequencies without any phase lags. At these locations, therefore, precipitation intensity appears to be modulated by the waves. However, there are also coherence peaks (not shown) at geographic locations where we do not expect African wave modulation of precipitation, so the interpretation of this evidence is somewhat uncertain. In a similar vein, Duvel (1990) also concluded that "wind and cloud spectral amplitudes are not [spatially] related in an obvious way. . . ."

c. Wave composites

Two sets of wave composites were constructed for two different longitudes, 2.5°W and 7.5°E, for the first and second halves of the season based on all six runs. For each of the two composites at the reference latitude 16°N, time series of the 890-mb "v" were filtered for

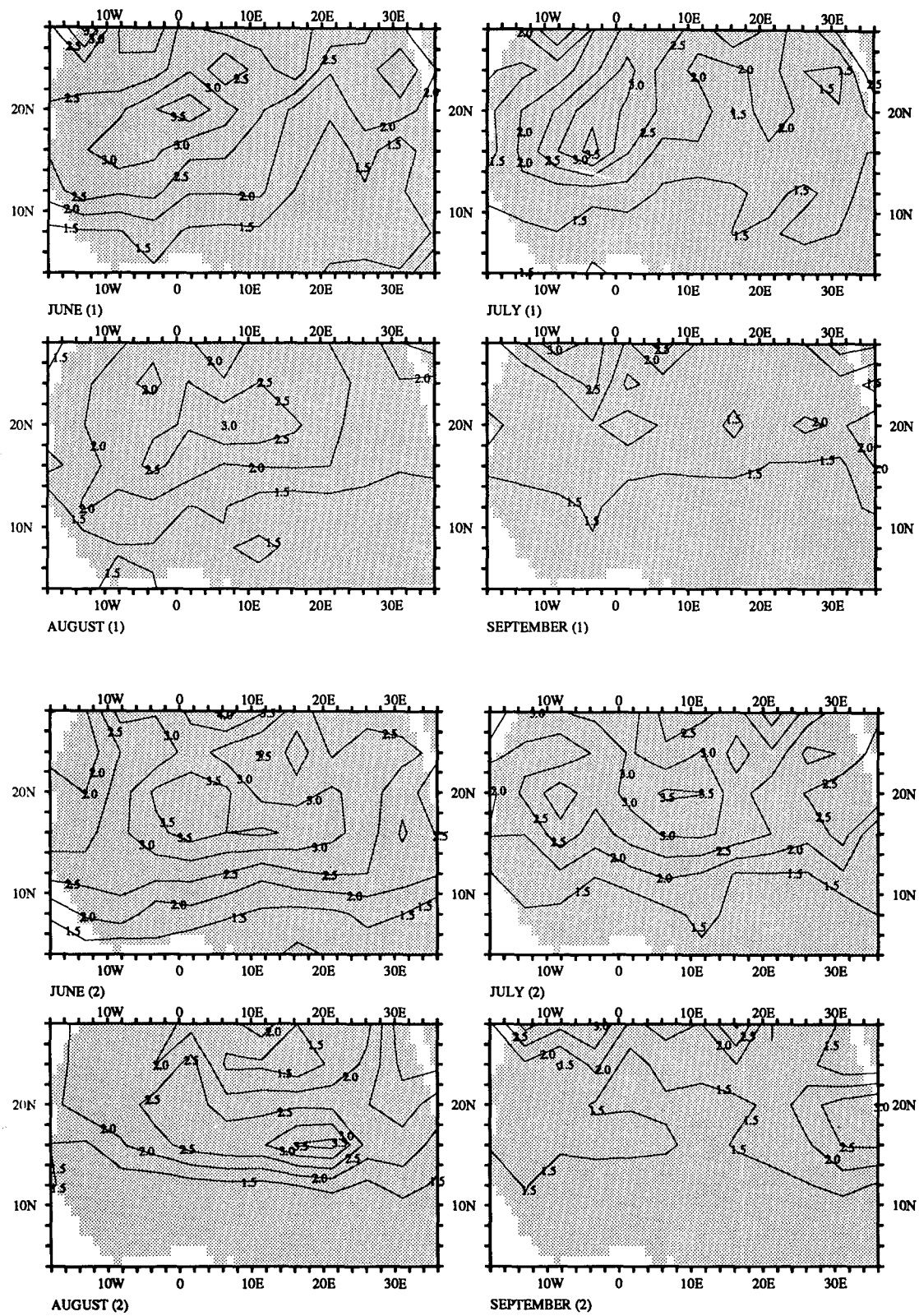

FIG. 7. Spatial distributions of the spectral amplitude of 780-mb meridional wind in the 5–8-day period band. Top: first ensemble; bottom: second ensemble (m s^{-1}).

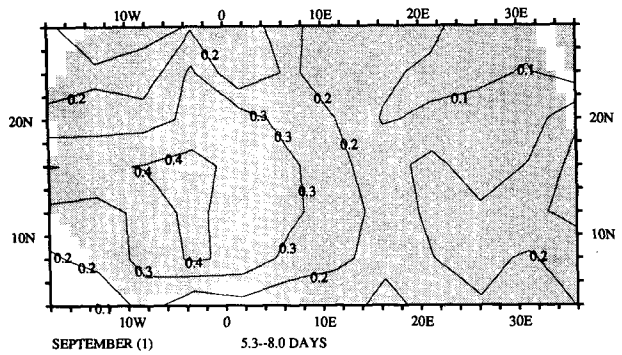

FIG. 8. Spatial distribution of the spectral power of 780-mb meridional wind integrated over the 5–8-day-period interval for September (first ensemble), expressed as a decimal fraction of power integrated over the entire spectrum.

the 5–8-day period band and were separated into discrete waves, defined by the consecutive maxima of v within each series. The wave segments were further divided into eight equal time intervals, representing different wave categories. Properties of composite waves were computed by averaging u, v, precipitation rate, and divergence for the same category interval over all waves in time series at each grid element along the same longitude. Wave composites of 890-mb wind vectors, precipitation rates, and divergence are shown in Fig. 12 where the maximum southerly wind at 16°N has been assigned to category 6.

The composites show cyclonic circulation, stronger during June–July than August–September (Figs. 12a,d,g,j), but otherwise similar to the spatial wave composites of 850-mb winds given by Reed et al. (1977). The divergence field at 2.5°W is quite strong in June–July (Fig. 12b) and compares favorably with the Reed et al. (1977) composite in that strong convergence is indicated west of the wave axis (category 2) and strong divergence east of the wave axis (category 6). Weaker versions of this composite are obtained at 7.5°E for both parts of the season (Figs. 12h,k). Only very weak convergence is associated with the August–September composite at 2.5°W (Fig. 12e), however.

June–July precipitation along 2.5°W is confined to the extreme southern edge of the wave composite (Fig. 12c). The small bumps in the 1–2 mm day^{-1} isohyets at categories 2 and 6 may indicate a marginal preference for rainfall at the convergence maximum and at the maximum southerly winds. At the same longitude during the second half of the season (Fig. 12f), heavier precipitation has moved northward to the latitudes of the composite wave. A prominent peak in the precipitation rates occurs at category 6 corresponding to the strongest southerly flow of the wave composite. A slight maximum at category 2 may be related to the weak convergence.

At 7.5°E, precipitation has already reached 16°N by June–July (Fig. 12i), and rates are lower west of the trough than elsewhere. During August–September (Fig. 12l), category 6, with its strong southerly winds, contains the maximum rainfall at most latitudes with a secondary maximum at category 3 (near the wave axis).

The slight preference for rainfall at the southerly wind maximum category is also present in several examples shown in Fig. 3. This wave modulation of the precipitation resembles Burpee's (1974) composites north of 12.5°N and Duvel's (1990) composite near 17.5°N. Simulations of African wave disturbances by a limited-area, 10-level, linearized primitive equation model (Mass 1979) are also relevant. They produced a precipitation maximum west of the wave trough near 9°N, which shifted to the east of the trough north of about 12°N. Our results do not show a clear association of modeled precipitation maxima with convergence maxima, as in the Reed et al. (1977) composite or Duvel's (1990) composite for waves near 7.5°N. Rather, most of the strong wave-induced convergence seems to occur north of the humid zone in air too dry to promote convective rainfall.

6. Discussion and conclusions

While GCM simulations in general do not always faithfully reproduce certain details of the observed climate, many important features of the African summer monsoon system are captured by the GISS GCM. Research that relies on the very sparse distribution of upper wind stations in the Sahel region must employ imaginative spatial interpolations that may not offer a complete or accurate picture of the daily fluctuations of circulation and rainfall. GCM studies complement observational investigations in that they provide complete four-dimensional (spatial and temporal) coverage

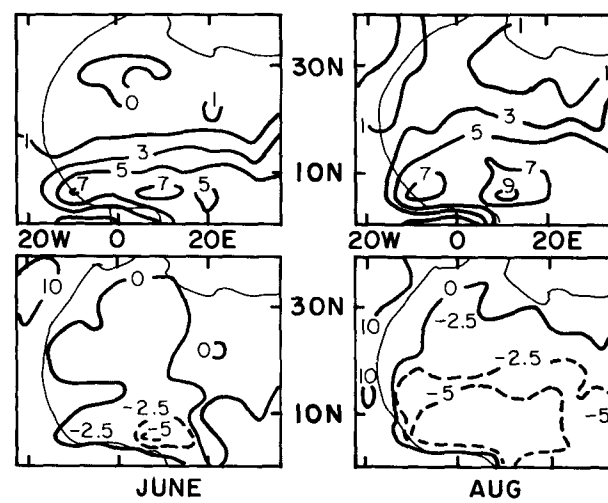

FIG. 9. (a,b) Mean precipitation rates for the first ensemble (mm day^{-1}). (c,d) Divergence of the vertical sum of horizontal moisture flux (in mm of precipitable water per month).

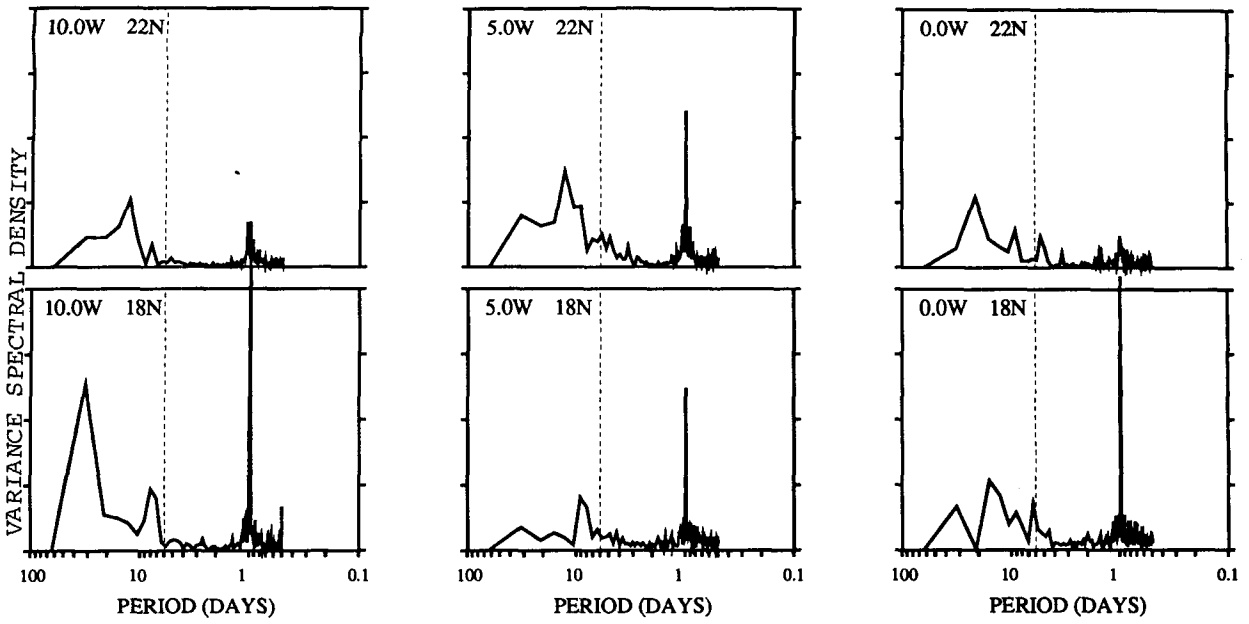

FIG. 10. Power spectra of 6-hourly mean precipitation rate, August–September of first ensemble. The reference line indicates 6-day periods.

of all of the relevant atmospheric variables and processes based on data given at each point of the model's uniformly spaced grid lattice.

The GISS GCM, run at a horizontal grid resolution of 4° by 5°, is shown to generate wavelike perturbations in the circulation of its lower troposphere, which share some of the characteristics of observed African wave disturbances over northern Africa. Modeled waves exhibit a realistic wavelength of about 2200 km, but propagate westward more slowly than observed, with

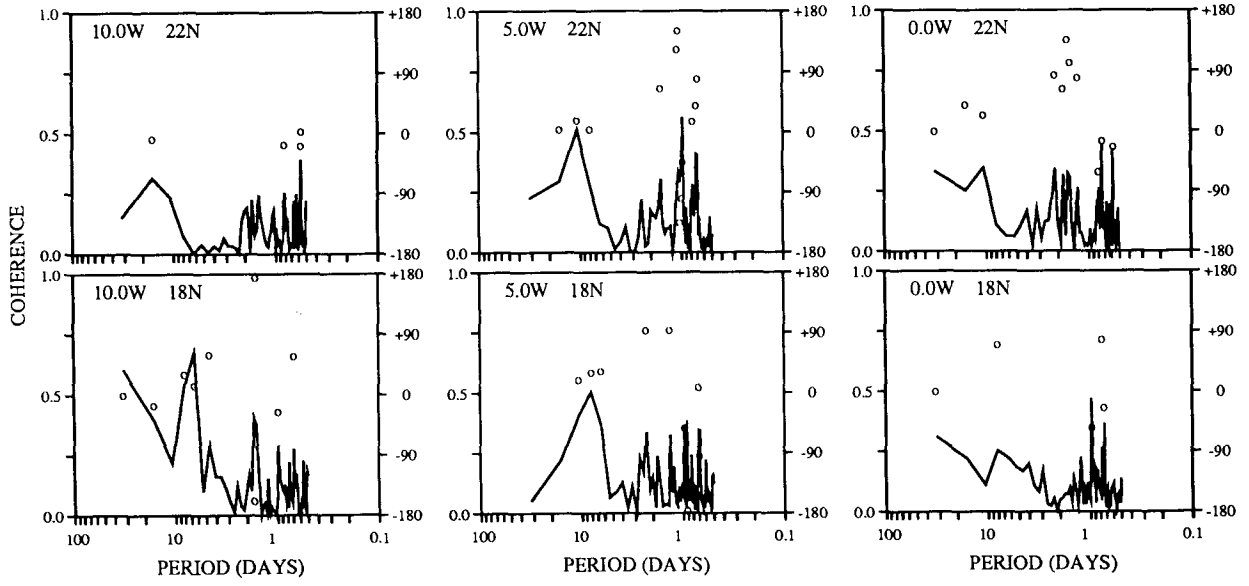

FIG. 11. Coherence spectra between 6-hourly mean 780-mb meridional winds (v) and 6-hourly mean precipitation rate, August–September. Circles indicate the relative phase at a particular period, plotted (for coherence >0.25) according to the right-hand scales. Spectra are averages based on 12 months of model simulations.

periods of 5–10 days, rather than the estimated 3–4-day periods implied by observational studies. Modeled mean zonal winds above northern Africa meet the Charney and Stern (1962) criterion for barotropic and baroclinic instability thought to be responsible for waves' initial growth during each of the (June–September) months of the simulations. Core speeds within the midtropospheric easterly jet are somewhat too weak, however, accounting for low propagation speeds of the simulated waves, especially during August.

The strongest wave amplitudes in these GCM simulations occur over West Africa during the first half of the summer. Nevertheless, 5–8-day-period waves still account for a large proportion of the September variance of midtropospheric meridional winds over a wide swath of West Africa, even though the spatial concentration of high wave amplitudes disappears after August. This occurs because September wave activity moves southward, where the total variance of these winds over the entire spectrum is relatively small in September, despite the strong AEJ. We have not isolated the cause of the low variance of midtropospheric meridional winds during September in the GCM. Modeled wave amplitudes are also unrealistically weak near the Atlantic coast throughout the season. Observed wave activity between 10° and 15°W may be related to the release of latent heat in organized convection (Norquist et al. 1977). We do not know whether the model's parameterization of convective rainfall dampens or intensifies simulated waves. In any case, the simulations show rather sparse rainfall along the Atlantic coast (compared with climatology) during the height of the monsoon season.

In both the model results and in several empirical studies, waves and associated convergences are fairly weak south of 10°N. Based on our study of composites of the simulated African wave disturbances, there is strong evidence of wave modulation of low-level convergence. Convergence at 890 mb is strongest in the wave category with northerly winds west of the trough. The spectral analysis shows that modeled precipitation is timed with the passage of waves at several locations. Some wave modulation of the modeled rainfall rates is also apparent from the August–September composites (Fig. 12), which show evidence of enhanced rainfall east of wave troughs, apparently in response to moisture advection by the southerly winds. The western side of the troughs, corresponding to northerly winds, is not the preferred location for the greatest rainfall, despite the convergence maxima. Moreover, the weakening of wave amplitudes and the weakening of the associated convergence/divergence in areas of strong convective precipitation suggest a negative association.

Wave composites constructed from observational data have shown that the relative frequencies of deep convection within the several wave categories do not conform to one morphology, and there are suggestions that the configuration may be influenced by season, latitude, or larger-scale dynamics (Burpee 1974; Payne and McGarry 1977; Chen and Ogura 1982; Duvel 1990). Nevertheless, the mutual exclusivity of strong wave activity and areas with deep moist convection in the GCM requires additional attention.

Model II allows a strong vertical mixing of horizontal momentum to accompany moist convection. Previous experience with the GCM has found that this lessens vertical wind shears and thus weakens the instability mechanism for wave formation (Rind 1993, personal communication). Over the Sahel, the upward mixing of near-surface westerly momentum probably also slows the midtropospheric easterlies wherever moist convection couples these layers, and presumably this also inhibits the growth of waves in the easterlies. Additional work is needed to clarify the influence of the vertical mixing of momentum by convection on modeled African waves and their modulation of precipitation.

We have described the basic properties of African wave disturbances in the GISS GCM and their associated circulations, as well as a weak modulation of rainfall that was not spatially correlated with the waves' low-level convergence zones. Although the simulated waves differ from observations in several details our results suggest that they introduce an important component of variability to the model's mean climate, which also occurs in nature. In addition, the present study provides a baseline to which the effects of improving model physics and resolution can be compared. We expect that changes in several model parameterizations (such as moist covection) that are currently being tested and an increase of horizontal grid resolution will yield more realistic morphologies of the modeled rainfall pattern associated with the waves. Better spatial organization of latent heat release and a better definition of the midtropospheric easterly jet could, in turn, also have beneficial effects on the dynamics of the modeled waves.

Global climate models have been effectively used to test the influence of SST patterns on the Sahel's interannual rainfall variability. African waves may well be an intermediate mechanism in this teleconnection, as they are known to modulate Sahel precipitation rates. This modeling study represents the first documentation of African wave disturbances in a GCM dedicated to climate research. By establishing the existence of African waves and their effect on rainfall rates in the GCM, we have given attention to a significant source of climate variability in the Sahel. Our results suggest that future GCM studies of the Sahel's climate will be more comprehensive if they consider the role of the African wave phenomenon.

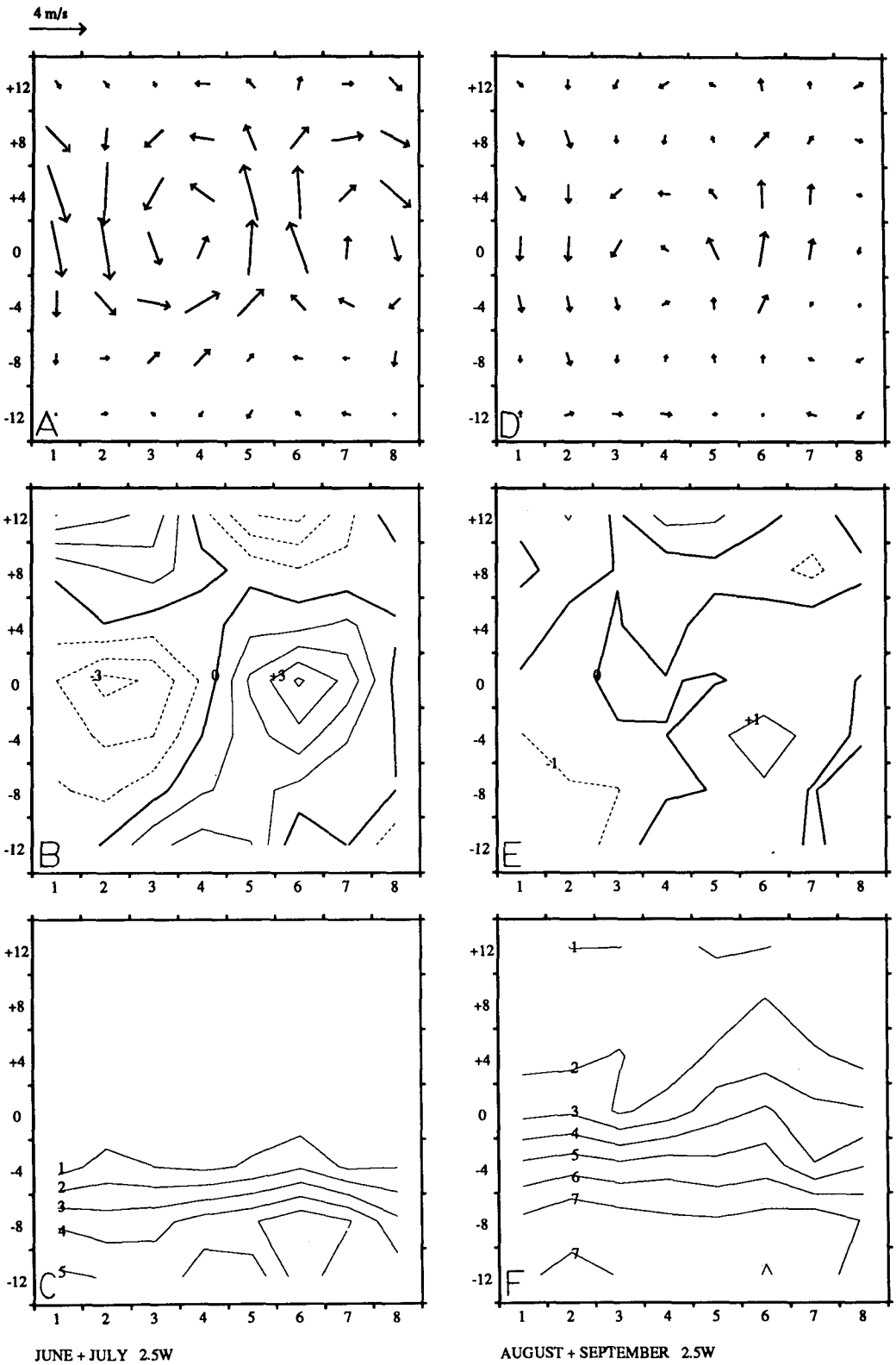

FIG. 12. Composite waves (see text): (a) along 2.5°W, (b) along 7.5°E, for the first (left) and second (right) halves of the season. Top: 890-mb wind vectors; middle: divergence of the 890-mb wind (10^{-6} sec^{-1}); bottom: precipitation rate (mm day^{-1}).

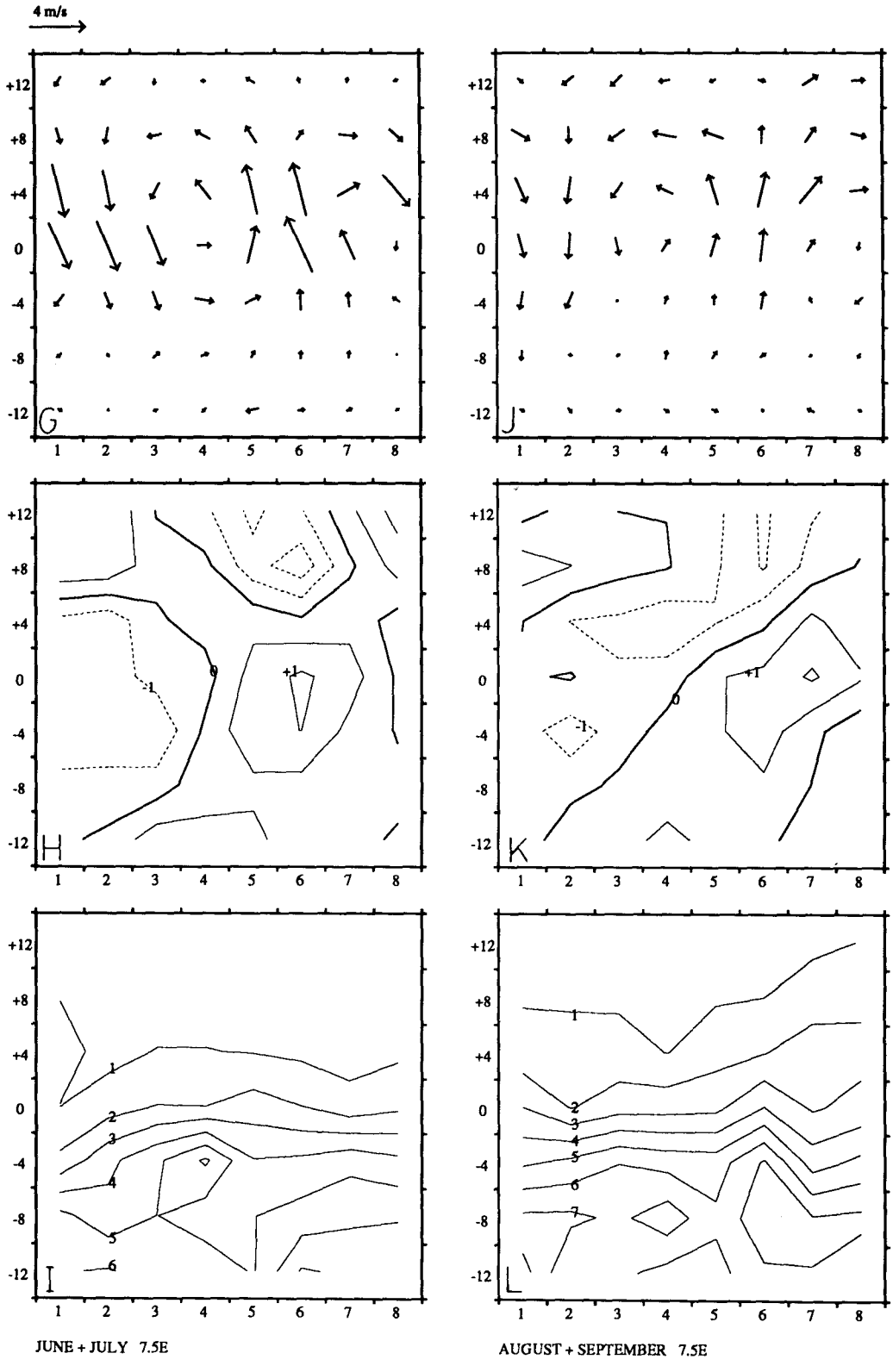

FIG. 12. (*Continued*)

Acknowledgments. This research was supported by DOE Grant DE-FG02-92ER61477 (LD), the NASA Atmospheric Chemistry Modeling and Analysis Program (TH), and the NASA Climate and Earth Observing System programs. We gratefully acknowledge encouragement and advice offered by Dr. D. Rind and helpful suggestions by anonymous reviewers. We are indebted to Dr. R. Miller, Cambridge, MA 02138, who shared his expertise with us in numerous consultations. Dr. P. Lonergan and C. J. Morris provided very able assistance in data processing.

REFERENCES

Albignat, J. P., and R. J. Reed, 1980: The origin of African wave disturbances during Phase III of GATE. *Mon. Wea. Rev.*, **108,** 1827–1839.

Burpee, R. W., 1971: The origin and structure of easterly waves in the lower troposphere of North Africa. PhD thesis, Department of Meteorology, Massachusetts Institute of Technology, 100 pp.

——, 1972: The origin and structure of easterly waves in the lower troposphere of North Africa. *J. Atmos. Sci.*, **29,** 77–90.

——, 1974: Characteristics of North African easterly waves during the summers of 1968 and 1969. *J. Atmos. Sci.*, **31,** 1556–1570.

Charney, J. G., and M. E. Stern, 1962: On the stability of internal baroclinic jets in a rotating atmosphere. *J. Atmos. Sci.*, **19,** 159–172.

Chen, Y., and Y. Ogura, 1982: Modulation of convective activity by large-scale flow patterns observed in GATE. *J. Atmos. Sci.*, **39,** 1260–1279.

Del Genio, A., and M. Yao, 1993: Efficient cumulus parameterization for long-term climate studies: The GISS scheme. *Cumulus Parameterization,* K. Emanuel and D. Raymond, Eds., AMS Monograph Series, in press.

Druyan, L. M., 1987: GCM studies of the African summer monsoon. *Climate Dyn.*, **2,** 117–126.

——, 1989: Advances in the study of sub-Saharan drought. *Int. J. Climatol.*, **9,** 77–90.

——, 1991: The sensitivity of sub-Saharan precipitation to Atlantic SST. *Clim. Change,* **18,** 17–36.

——, 1992: Tropical impacts of 1987/1988 SST on GISS GCM climate simulations. Simulation of Interannual and Intraseasonal Monsoon Variability, (Report of NCAR workshop, WCRP-68, World Meteorological Organization, Geneva, 2.25–2.29.

——, and D. Rind, 1989: *Verification of Regional Climates of GISS GCM-Part 2: Summer,* NASA Tech. Memo. 100722, 39 pp. [Available from GSFC, Greenbelt, MD 20771.]

Duvel, J. P., 1988: Analysis of diurnal, interdiurnal and interannual variations during Northern Hemisphere summers using Meteosat infrared channels. *J. Climate,* **1,** 471–484.

——, 1990: Convection over tropical Africa and the Atlantic Ocean during northern summer. Part II: Modulation by easterly waves. *Mon. Wea. Rev.*, **118,** 1855–1868.

Fortune, M., 1980: Properties of African squall lines inferred from time-lapse satellite imagery. *Mon. Wea. Rev.*, **108,** 153–168.

Hansen, J., G., Russell, D. Rind, P. Stone, A. Lacis, S. Lebedeff, R. Ruedy, and L. Travis, 1983: Efficient three-dimensional global models for climate studies: Models I and II. *Mon. Wea. Rev.*, **111,** 609–662.

Hastenrath, S., 1988: *Climate and Circulation of the Tropics,* D. Reidel Pub. 455 pp.

Kidson, J. W., 1977: African rainfall and its relation to the upper air circulation. *Quart. J. Roy. Meteor. Soc.*, **103,** 441–456.

Kwon, H. J., 1989: A reexamination of the genesis of African waves. *J. Atmos. Sci.*, **46,** 3621–3631.

Lamb, P. J., and R. A. Peppler, 1991: West Africa. *Teleconnections: Linkages Between ENSO, Worldwide Climate Anomalies, and Societal Impacts,* M. H. Glantz, R. W. Katz, and N. Nicholls, Eds., Cambridge University Press, 121–189.

——, and ——, 1992: Further case studies of tropical Atlantic surface atmospheric and oceanic patterns associated with sub-Saharan drought. *J. Climate,* **5,** 476–488.

Landsea, C. W., and W. M. Gray, 1992: The strong association between western Sahelian monsoon rainfall and intense Atlantic hurricanes. *J. Climate,* **5,** 435–453.

Mass, C., 1979: A linear primitive equation model of African wave disturbances. *J. Atmos. Sci.*, **36,** 2075–2092.

Miller, R. L., and R. S. Lindzen, 1992: Organization of rainfall by an unstable jet with an application to African waves. *J. Atmos. Sci.*, **49,** 1523–1554.

Miyakoda, K., and J. Sirutis, 1977: Comparative integrations of global models with various parameterized processes of subgrid-scale vertical transports: description of the parameterizations. *Beitr. Phys. der Atmos.*, **50,** 445–487.

Newell, R. E., and J. W. Kidson, 1984: African mean wind changes between Sahelian wet and dry periods. *J. Climatol.*, **4,** 27–33.

Norquist, D. C., E. E. Recker, and R. J. Reed, 1977: The energetics of African wave disturbances as observed during Phase III of GATE. *Mon. Wea. Rev.*, **105,** 334–342.

Payne, S. W., and M. M. McGarry, 1977: The relationship of satellite convective activity to easterly waves over West Africa and the adjacent ocean during Phase III of GATE. *Mon. Wea. Rev.*, **105,** 413–420.

Ratcliffe, R., 1989a: Northern Hemisphere circulation review. *Int. J. Climatol.*, **9,** 106–109.

——, 1989b: Northern Hemisphere circulation review. *Int. J. Climatol.*, **9,** 546–549.

Reed, R. J., D. C. Norquist, and E. E. Recker, 1977: The structure and properties of African wave disturbances as observed during Phase III of GATE. *Mon. Wea. Rev.*, **105,** 317–333.

——, A. Hollingsworth, W. A. Heckley, and F. Delsol, 1988: An evaluation of the performance of the ECMWF operational system in analyzing and forecasting easterly wave disturbances over Africa and the tropical Atlantic. *Mon. Wea. Rev.*, **116,** 824–865.

Rind, D., 1987: The doubled CO_2 climate: Impact of the SST gradient. *J. Atmos. Sci.*, **44,** 3235–3268.

——, 1988: Dependence of warm and cold climate depiction on climate model resolution. *J. Climate,* **1,** 965–997.

Rowell, D. P., C. K. Folland, and K. Maskell, J. A. Owen, and M. N. Ward, 1992: Modelling the influence of global SST on the variability and predictability of seasonal Sahel rainfall. *Geophys. Res. Lett.*, **19,** 905–908.

World Meteorological Organization, 1985: *The Global Climate System—A Critical Review of the Climate System During 1982–1984.* World Climate Data Program, WMO, 52 pp.